Q-Factor Estimation via Convolutional Seismic Modeling

Leandro R. S. Farias, Tales V. R. O. Câmara, Luiz F. Q. Silveira, Kenji Nose-Filho, and Tiago Barros

***Abstract*— This work presents a method for estimating the seismic quality factor from surface reflection data by solving an inverse problem based on the convolutional model. Using gradient descent to minimize the mean square error between observed and modeled traces, the approach allows flexible attenuation modeling, with one of its key features being the interchangeability of the assumed attenuation model. Synthetic tests with known source and reflectivity demonstrate accurate trace reconstruction, supporting the method's potential integration into seismic processing workflows. The study also analyzes the effects of model mismatch by generating data with one attenuation model and inverting it using another.**

***Keywords*— Quality factor, inverse problem, convolutional model, seismic attenuation.**

I. Introduction

The anelasticity and inhomogeneity of seismic media give rise to two primary phenomena: energy dissipation and velocity dispersion. Dissipation, characterized by a reduction in the amplitude of the seismic wavelet, occurs as energy is lost from the wavelet to the medium. Velocity dispersion, on the other hand, is characterized by the broadening and delaying of the wavelet, causing variations in the wavelet's phase along the travel path [1]. These two effects are intrinsically linked and are described by the Earth's quality factor, Q.

To obtain high-resolution seismic images, accurate treatment of both dissipation and dispersion is essential. Consequently, wave-propagation reversal procedures, such as inverse Q filtering, are applied. For these methods to be effective, an accurate estimation of the subsurface Q-factor is required. While most existing techniques rely on Vertical Seismic Profile (VSP) data [2], estimating Q directly from surface reflection data is often more practical and widely applicable. Numerous studies have been dedicated to seismic attenuation estimation using a variety of approaches and data types, including enhanced log spectral ratio methods [3], interferometric techniques with VSP data [4], and time-frequency transforms [5].

This work presents a method for estimating the Q-factor from surface reflection data by formulating an inverse problem based on the seismic convolutional model [6]. Unlike conventional approaches, our method directly parameterizes the convolutional model and adjusts its parameters so that the synthetic trace fits the observed reflection data. The solution is obtained using gradient descent to minimize a squared error cost function. A key advantage of this approach lies in its flexibility: it allows for easy substitution of different attenuation models within the same inversion framework. Furthermore, we explore the influence of attenuation model selection by generating synthetic data with one model and attempting to recover Q using a different one — highlighting the practical implications of model mismatch in Q estimation. This dual contribution strengthens the method's relevance for inversion applications and provides insights into the robustness of attenuation assumptions in seismic workflows.

The remainder of this paper is organized as follows: Section II presents the theoretical background. Section III describes the formulation of the inverse problem and the gradient-based algorithm used for Q-factor estimation. Section IV presents numerical results for synthetic data generated using multiple attenuation models. In Section V, the impact of model mismatch on the estimation accuracy is discussed. Finally, Section VI provides the main conclusions and outlines directions for future work.

II. Theory

A. Convolutional model formulation

According to Ergun [7], seismic data $x(t)$ can be described as the convolution of the seismic source wavelet $s(t)$ with the reflectivity series of the medium $r(t)$, given by:

$$x(t) = s(t) * r(t) = \int_{\mathbb{R}} s(t-\tau)\, r(\tau)\, \mathrm{d}\tau, \tag{1}$$

where the symbol $*$ denotes the continuous-time convolution between the two signals.

In numerical computations, this operation is discretized using a sampling period Δt and expressed as a matrix-vector multiplication:

$$\mathbf{x} = \mathbf{S}\mathbf{r}, \tag{2}$$

where $\mathbf{r}$ is a column vector representing the discrete reflectivity series:

$$\mathbf{r} = \begin{bmatrix} r(0) & r(\Delta t) & r(2\Delta t) & \dots & r((N_r-1)\Delta t) \end{bmatrix}^T, \tag{3}$$

and $\mathbf{s}$ is a column vector formed from the discretized source wavelet:

$$\mathbf{s} = \begin{bmatrix} s(0) & s(\Delta t) & s(2\Delta t) & \dots & s((N_s-1)\Delta t) \end{bmatrix}^T. \tag{4}$$

Leandro R. S. Farias, Tales V. R. O. Câmara, Luiz F. Q. Silveira, and Tiago Barros are with the Universidade Federal do Rio Grande do Norte (UFRN), Natal–RN, Brazil. Kenji Nose-Filho is with the Universidade Federal do ABC (UFABC), Santo André–SP, Brazil. E-mails: leandro.farias.highres@imd.ufrn.br, talescamara@gmail.com, lfelipe@dca.ufrn.br, tbarros@dca.ufrn.br, kenjinose@gmail.com. This work was supported by Equinor.

The matrix $\mathbf{S}$ is a Toeplitz matrix of size $(N_r + N_s - 1) \times N_r$, constructed by shifting the source wavelet $\mathbf{s}$ along its columns:

$$\mathbf{S} = \begin{bmatrix} s(0) & 0 & 0 & \cdots & 0 \\ s(1) & s(0) & 0 & \cdots & 0 \\ \vdots & \ddots & \ddots & \ddots & \vdots \\ 0 & \cdots & s(1) & s(0) & 0 \\ 0 & \cdots & s(2) & s(1) & s(0) \\ \vdots & \cdots & \cdots & \ddots & \vdots \\ 0 & \cdots & \cdots & \cdots & s(N_s-1) \end{bmatrix}. \quad (5)$$

This formulation assumes the seismic wavelet remains unchanged during propagation (i.e., the source vector is simply repeated across the columns of $\mathbf{S}$). In practice, however, energy dissipation and velocity dispersion alter the wavelet's amplitude and shape as it propagates [1]. To account for these effects, Ergun [7] proposed introducing a non-stationary function $a(t, \tau)$ in Eq. (1), such that:

$$x(t) = s(t) * a(t,\tau) \odot r(t) = s(t) * \int_{\mathbb{R}} a(t-\tau, \tau)\, r(\tau)\, \mathrm{d}\tau, \quad (6)$$

where $\odot$ is the non-stationary convolution operation, and τ is the wave's travel time in the seismic medium. The discrete counterpart of Eq. (6) is

$$\mathbf{x} = \mathbf{SAr}, \quad (7)$$

where $\mathbf{A}$ is called the attenuation matrix, with size $N_r \times N_r$, whose construction is described in the next subsection.

B. Assembly of the attenuation matrix

To construct the attenuation matrix, a one-dimensional seismic medium is considered, with depth represented by the variable z. Assuming the medium to be linear, the solutions of the wave equation can be described as a superposition of plane waves with fixed angular frequency ω [8]. As a result, the wave amplitude at depth z and time t is given by

$$u(z,t) = \int_{\mathbb{R}} S(\omega) \exp\left[i\omega t - ik(z,\omega)z\right] \mathrm{d}\omega, \quad (8)$$

where $S(\omega)$ is the spectral amplitude of the source wavelet at the surface, and $k(z, \omega)$ is the wavenumber, dependent on both depth and frequency. This expression can also be written as an inverse Fourier transform:

$$u(z,t) = \mathcal{F}^{-1}\left\{S(\omega) \exp\left[-ik(z,\omega)z\right]\right\}. \quad (9)$$

To express the wavefield as a function of travel time τ instead of depth z, the medium is divided into layers of thickness Δz_n, where n indexes each layer, such that:

$$\Delta z_n = v_n(\omega_r)\Delta\tau, \quad (10)$$

where $v_n(\omega_r)$ is the phase velocity at the n-th layer, assessed at a reference frequency ω_r, typically chosen as the central frequency of the wavelet [9], and $\Delta\tau$ is the fixed travel-time step. For simplicity of notation, the wave amplitude at the n-th layer is denoted $u_n(t)$, and the wavenumber as $k_n(\omega)$. Then, the convolution property of the Fourier transform can be applied to Eq. (9), leading to the following expression:

$$u_n(t) = s(t) * a_n(t), \quad (11)$$

where:

$$a_n(t) = \mathcal{F}^{-1}\left\{\exp\left[-i\Delta\tau \sum_{j=1}^{n} k_j(\omega) v_j(\omega_r)\right]\right\}. \quad (12)$$

This function describes how the source wavelet $s(t)$ is attenuated upon reaching the n-th layer. To account for the attenuation across all layers, the attenuation matrix is defined as follows:

$$\mathbf{A} = \begin{bmatrix} \mathbf{a}_0 & \mathbf{a}_1 & \mathbf{a}_2 \cdots & \mathbf{a}_{N_r-1} \end{bmatrix}, \quad (13)$$

where each column vector $\mathbf{a}_n$ is obtained by discretizing $a_n(t)$:

$$\mathbf{a}_n = \begin{bmatrix} a_n(0) & a_n(\Delta t) & \ldots & a_n((N_r-1)\Delta t) \end{bmatrix}^T. \quad (14)$$

In this way, multiplying $\mathbf{S}$ by $\mathbf{A}$ yields a matrix whose columns represent the attenuated wavelet at each layer of the medium.

C. Choice of an attenuation model

According to Ursin [10], the wavenumber is a complex quantity that combines the frequency-dependent phase velocity $v_n(\omega)$ and the attenuation coefficient $\alpha_n(\omega)$ in the n-th layer of the medium in the following way:

$$k_n(\omega) = \frac{|\omega|}{v_n(\omega)} - i\alpha_n(\omega). \quad (15)$$

The models for the Earth Q-factor behavior are defined by mathematical expressions for these two quantities. The widely-used Kolsky-Futterman (KF) model [11], with proper parameter adjustment, can behave similarly to most of the models used in seismic data processing [10]. For this reason, the KF model was chosen for modeling the attenuation matrix in this work, although another model can be easily used by choosing the proper $v_n(\omega)$ and $\alpha_n(\omega)$ expressions. For the purposes of this work, the Q-factor is considered to be uniform through the propagation medium, meaning that it does not vary with z or τ.

The mathematical definitions for the KF model at the n-th layer are

$$\alpha_n(\omega) = \frac{|\omega|}{2v_n(\omega_r)Q(\omega_r)}, \quad (16)$$

$$\frac{1}{v_n(\omega)} = \frac{1}{v_n(\omega_r)} - \frac{1}{\pi v_n(\omega_r)Q(\omega_r)} \ln\left|\frac{\omega}{\omega_r}\right|. \quad (17)$$

Replacing these two expressions in Eq. (15), and then the result in Eq. (12), the expression for the n-th column of the attenuation matrix becomes

$$a_n(t) = \mathcal{F}^{-1}\left\{f_{n,\text{disp}}(\omega) f_{n,\text{diss}}(\omega)\right\}, \quad (18)$$

where $f_{n,\text{disp}}$ is a function modeling the velocity dispersion effect on the wave propagation at the n-th layer, characterized by a modification in phase,

$$f_{n,\text{disp}}(\omega) = \exp\left[-in\Delta\tau\left(|\omega| - \frac{|\omega|}{\pi Q(\omega_r)}\ln\left|\frac{\omega}{\omega_r}\right|\right)\right], \quad (19)$$

and $f_{n,\text{diss}}$ is a function modeling the dissipation of energy during wave propagation at n-th layer, characterized by a reduction of amplitude,

$$f_{n,\text{diss}}(\omega) = \exp\left[-\frac{|\omega|n\Delta\tau}{2Q(\omega_r)}\right]. \quad (20)$$

It is worth noting that, if $Q(\omega_r) \to \infty$, indicating a lossless medium, it follows that:

$$a_n(t) = \mathcal{F}^{-1}\left\{\exp[-i|\omega|n\Delta\tau]\right\} = \delta(t - n\Delta\tau). \quad (21)$$

This implies that $\mathbf{A}$ becomes the identity matrix, which is consistent with the expected behavior of a lossless medium.

III. Method

A. Cost function definition

Given the analytical expression for the attenuation matrix calculation, the inverse problem of estimating the Q-factor can be formulated as a cost function minimization problem

$$\min_{Q} J(Q). \quad (22)$$

In this work, a quadratic loss function was adopted:

$$J(Q) = \frac{1}{2}\sum_{m=0}^{N_r+N_s-2}\left([\mathbf{SAr}]_m - x_{\text{obs},m}\right)^2, \quad (23)$$

where $\mathbf{x_{obs}}$ represents the observed seismic trace, and $Q = Q(\omega_r)$ is the quality factor evaluated at the reference frequency ω_r. It is important to recall that the only factor that varies with Q in Eq. (23) is the matrix $\mathbf{A}$.

B. Gradient descent algorithm

In order to minimize the cost function described at Eq. (23), the gradient descent algorithm can be employed. In this context, the quality factor at the k-th iteration is updated as follows:

$$Q_{k+1} = Q_k - \eta\frac{\partial J(Q)}{\partial Q}\bigg|_{Q=Q_k}, \quad (24)$$

where η is the learning rate hyperparameter. The derivative $\frac{\partial J(Q)}{\partial Q}$ can be analytically obtained, as shown below:

$$\frac{\partial J(Q)}{\partial Q} = \sum_{m=1}^{N_r+N_s-2}\left([\mathbf{SAr}]_m - x_{\text{obs},m}\right)\left[\mathbf{S}\frac{\partial \mathbf{A}}{\partial Q}\mathbf{r}\right]_m, \quad (25)$$

where the derivative $\frac{\partial \mathbf{A}}{\partial Q}$ is calculated for each column of the matrix $\mathbf{A}$, resulting in

$$\frac{\partial a_n(t)}{\partial Q} = \frac{n\Delta\tau}{Q^2}\mathcal{F}^{-1}\left\{|\omega|A_n(\omega)\left(\frac{1}{2} - i\frac{1}{\pi}\ln\left|\frac{\omega}{\omega_r}\right|\right)\right\}, \quad (26)$$

where $A_n(\omega)$ is the expression inside the brackets of Eq. (18).

C. Adaptive learning rate

During initial tests, it was observed that the algorithm struggled to converge because the gradient step became too small due to the Q^2 term in the denominator. A practical modification to the optimization process is the use of an adaptive learning rate η'_k, defined as:

$$\eta'_k := \eta Q_k^2, \quad (27)$$

This adaptation ensures that, for higher values of Q, the gradient descent step is properly scaled. As a result, Eq. (24) can be rewritten as

$$Q_{k+1} = Q_k - \eta'_k\frac{\partial J(Q)}{\partial Q}\bigg|_{Q=Q_k}. \quad (28)$$

IV. Results

A. Test scenario

To evaluate the performance of the Q estimation algorithm, a one-dimensional seismic medium with a known source and reflectivity function was used, in order to focus on the quality factor estimation aspect of the process. The medium has a uniform quality factor of $Q_{true} = 25$, which serves as the benchmark for the estimation process. The source wavelet and reflectivity series of the scenario are presented in Figures 1 and 2, respectively.

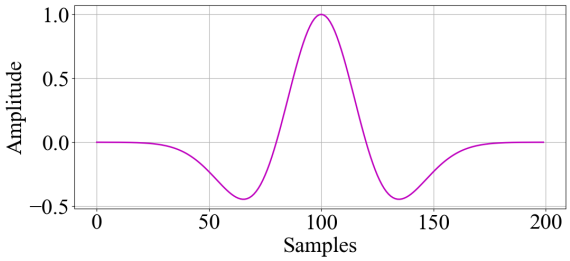

Fig. 1. Wavelet used for generating the synthetic seismic trace.

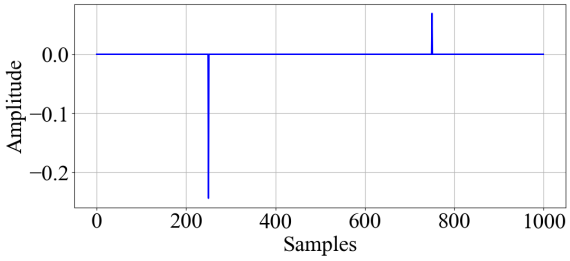

Fig. 2. Reflectivity series used for generating the synthetic seismic trace.

The observed seismic trace $\mathbf{x_{obs}}$ is generated using the non-stationary convolutional model in Eq. (7), with $\mathbf{S}$ and $\mathbf{r}$ being assembled based on the data presented in Figures 1 and 2, respectively. The attenuation matrix $\mathbf{A}$ is calculated using different Earth quality factor models, following the formulations described in [1] and [10]. The following Earth Q-factor models were used:

- **Azimi model:** characterized by a frequency-dependent attenuation coefficient that follows a power-law:

$$\alpha_n(\omega) = a\,|\omega|^{1-\beta}, \tag{29}$$

and a phase velocity given by:

$$\frac{1}{v_n(\omega)} = \frac{1}{v_n(\omega_r)} + a\,|\omega|^{-\beta}\cot\left(\frac{\pi}{2}\beta\right). \tag{30}$$

The parameters a and β are adjustable.

- **Kjartansson model:** assumes a constant quality factor across frequency, resulting in:

$$\alpha_n(\omega) = a\,|\omega|^{1-\beta}, \tag{31}$$

$$\frac{1}{v_n(\omega)} = a\,|\omega|^{-\beta}\cot\left(\frac{\pi}{2}\beta\right), \tag{32}$$

with a and β as tunable parameters.

- **Zener model:** known as the standard linear solid model, defined by:

$$\alpha_n(\omega) = \frac{\omega^2\tau_c}{v_n(\omega_r)Q_c(1+\omega^2\tau_c^2)}, \tag{33}$$

$$\frac{1}{v_n(\omega)} = \frac{1}{v_n(\omega_r)}\left[1 - \frac{\omega^2\tau_c^2}{Q_c(1+\omega^2\tau_c^2)}\right], \tag{34}$$

where τ_c and Q_c are the model's adjustable parameters.

In all cases, the adjustable parameters can be expressed as functions of the quality factor $Q(\omega_r)$ and the phase velocity $v_n(\omega_r)$, as shown by Ursin [10]. The KF model was also used to generated the data for an initial test of the Q-estimation algorithm. The resulting seismic traces are shown as the $\mathbf{x_{obs}}$ curves in Figures 3 to 6.

B. Q-factor estimation algorithm application

The gradient descent update described in Eq. (28) was applied to each synthetic dataset, starting from an initial guess of $Q_0 = 200$, which represents an almost lossless seismic environment. For each case, an estimated quality factor, $\hat{Q}$, was obtained. The results are illustrated in Figures 3 to 6, where three seismic traces are shown for comparison:

$$\mathbf{x_0} = \mathbf{S}\mathbf{A_0}\mathbf{r}, \tag{35}$$

corresponding to the synthetic trace generated using the attenuation matrix $\mathbf{A_0}$, built with the initial guess Q_0;

$$\hat{\mathbf{x}} = \mathbf{S}\hat{\mathbf{A}}\mathbf{r}, \tag{36}$$

representing the trace generated using the estimated attenuation matrix $\hat{\mathbf{A}}$, constructed from the final value $\hat{Q}$ obtained through the optimization process;

$$\mathbf{x_{obs}} = \mathbf{S}\mathbf{A_{obs}}\mathbf{r}, \tag{37}$$

which is the reference trace, generated using the true quality factor Q_{true} and its corresponding attenuation matrix $\mathbf{A_{obs}}$.

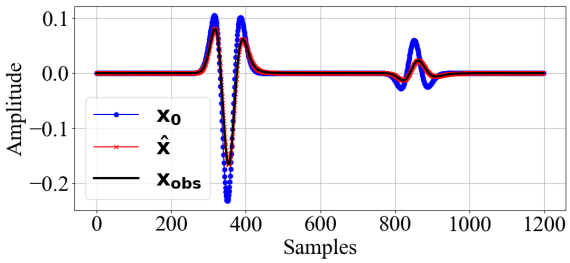

Fig. 3. Comparison between initial, estimated, and observed traces for data generated using KF's model.

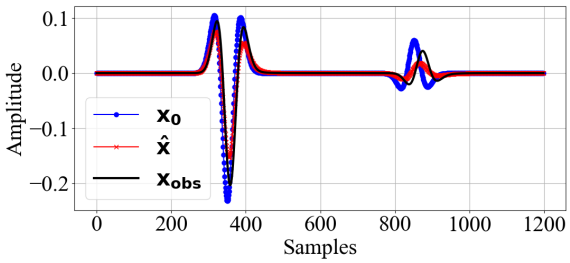

Fig. 4. Comparison between initial, estimated, and observed traces for data generated using Azimi's model.

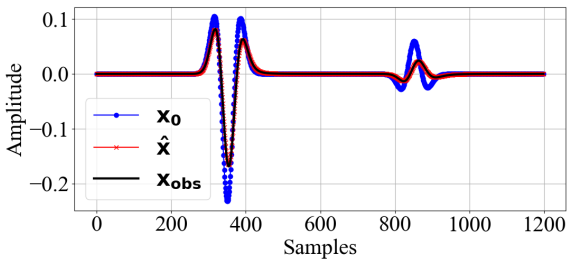

Fig. 5. Comparison between initial, estimated, and observed traces for data generated using Kjartansson's model.

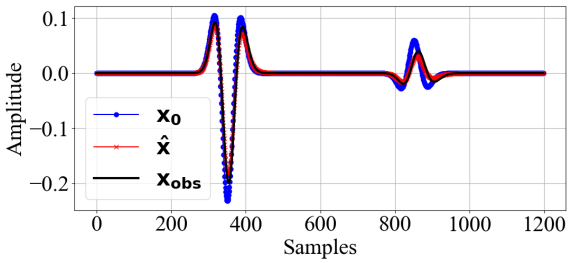

Fig. 6. Comparison between initial, estimated, and observed traces for data generated using Zener's model.

Table I presents the estimated quality factor $\hat{Q}$ obtained by the algorithm for each synthetic trace, along with the corresponding relative error in percentage. Each row corresponds to a different attenuation model used to generate the reference trace $\mathbf{x_{obs}}$, and the true quality factor used in all cases is $Q_{\text{true}} = 25$. The relative error is computed as the absolute difference between $\hat{Q}$ and Q_{true}, normalized by Q_{true}.

TABLE I
ESTIMATED QUALITY FACTORS $\hat{Q}$ AND RELATIVE ERRORS FOR EACH SYNTHETIC TRACE $\mathbf{x_{obs}}$. THE REFERENCE VALUE IS $Q_{true} = 25$.

Trace	Estimated Quality Factor $\hat{Q}$	Relative Error (%)
KF	25.00	0.00
Azimi	20.73	17.08
Kjartansson	24.91	0.36
Zener	34.87	39.48

V. DISCUSSIONS

In Figure 3, the estimation method—which uses the KF model as its inversion framework—is applied to data also generated with the KF model, thereby testing the method under the simplest condition. As expected, it accurately estimates the value $\hat{Q} = 25$ with 0% error, as presented in Table I, and the match between the estimated trace $\hat{\mathbf{x}}$ and the observed trace $\mathbf{x_{obs}}$ is perfect, demonstrating the effectiveness of the algorithm.

In a more complex scenario, the $\mathbf{x_{obs}}$ curve in Figure 4 is generated using Azimi's model. The results in the figure show that the optimization process successfully reduces the error between the initial estimate and the observed trace. However, the match between the estimated trace $\hat{\mathbf{x}}$ and the observed trace $\mathbf{x_{obs}}$ is not perfect. This discrepancy stems from the incompatibility between the Kolsky-Futterman and Azimi models, as discussed by Ursin [10]. Therefore, the estimated quality factor $\hat{Q} = 20.73$ presented in Table I represents the value that best minimizes the error for a trace originally generated using the Azimi model, even though a perfect match cannot be achieved.

In Figure 5, the data is generated using Kjartansson's model. In Table I, the estimated $\hat{Q}$ value is very close to the true value Q_{true}, with a relative error of 0.36%, and the fit between $\hat{\mathbf{x}}$ and $\mathbf{x_{obs}}$ is nearly perfect. This indicates that the cost function—Eq. (23)—approaches zero. Such accuracy is possible because the Kjartansson model can be closely represented within the Kolsky-Futterman framework, as shown by Ursin [10].

In contrast, the application of the estimation method to data generated using Zener's model (Figure 6) shows that, although the error between $\hat{Q}$ and Q_{true} is elevated (39.48%, as seen in Table I), the error between $\hat{\mathbf{x}}$ and $\mathbf{x_{obs}}$ remains small. This again reflects the incompatibility between the Zener and Kolsky-Futterman models, as discussed by Ursin [10]. Nevertheless, the estimated value $\hat{Q} = 34.87$ within the Kolsky-Futterman framework allows the synthetic trace to closely approximate the observed one, despite the discrepancy in Q values.

VI. CONCLUSIONS

This work proposed a flexible method for estimating the seismic quality factor Q from surface reflection data by solving an inverse problem based on the convolutional model. The proposed technique, which applies gradient descent to minimize the mismatch between observed and modeled traces, proved to be effective in reconstructing seismic waveforms, even when the exact value of Q was not recovered.

The results highlight that the estimated Q value is intrinsically linked to the chosen attenuation model rather than to a fixed physical property of the medium. As demonstrated in the Zener model case, even when the estimated Q value differs significantly from the actual one, the reconstructed trace can still closely match the observed data. This reinforces the notion that Q is model-dependent and must be interpreted accordingly.

Given its simplicity and flexibility, the proposed method shows strong potential for integration into seismic deconvolution workflows. Future work will explore the use of a non-uniform quality factor, enabling application to more realistic scenarios in which attenuation remains constant within each layer but varies across layers. This can be achieved by adapting the method to incorporate a vector of Q-factor values, one for each sub-layer, rather than relying on a single global value as done in this paper. We also plan to evaluate the method under more realistic conditions, including the presence of additive Gaussian and impulsive noise, to assess its robustness in practical settings. Ultimately, our goal is to apply the method to real field data to validate its performance in real-world scenarios.

ACKNOWLEDGMENTS

The authors gratefully acknowledge support from Equinor through the R&D project "Non-Stationary Deconvolution and Imaging for High-Resolution Seismic" and ANP for its strategic R&D levy regulation.

REFERENCES

[1] Y. Wang, "Inverse Q-filter for seismic resolution enhancement," *Geophysics*, vol. 71, no. 3, pp. V51–V60, 2006.

[2] P. Cheng and G. F. Margrave, "Estimation of Q: a comparison of different computational methods," *CREWES Research Report*, vol. 24, pp. 1–32, 2012.

[3] N. Liu, S. Wei, Y. Yang, S. Li, F. Sun, and J. Gao, "Seismic attenuation estimation using an enhanced log spectral ratio method," *IEEE Geoscience and Remote Sensing Letters*, vol. 19, pp. 1–5, 2022. doi: 10.1109/LGRS.2022.3140343.

[4] J. Matsushima, M. Y. Ali, and F. Bouchaala, "Seismic attenuation estimation from zero-offset VSP data using seismic interferometry," *Geophysical Journal International*, vol. 204, no. 2, pp. 1288–1307, 2015. doi: 10.1093/gji/ggv522.

[5] W. Liu, Z. Li, X. Huang, H. Qin, Y. Xie, K. Chen, and Z. Zhang, "Seismic attenuation parameter estimation based on improved GLCT," *IEEE Geoscience and Remote Sensing Letters*, vol. 21, pp. 1–5, 2024. doi: 10.1109/LGRS.2024.3477589.

[6] A. K. Takahata, E. Z. Nadalin, R. Ferrari, L. T. Duarte, R. Suyama, R. R. Lopes, J. M. T. Romano, and M. Tygel, "Unsupervised processing of geophysical signals: A review of some key aspects of blind deconvolution and blind source separation," *IEEE Signal Processing Magazine*, vol. 29, no. 4, pp. 27–35, 2012. DOI: 10.1109/MSP.2012.2189999.

[7] E. Ergun, *Non-stationary Iterative Time-Domain Deconvolution for Enhancing the Resolution of Shallow Seismic Data*, Master's thesis, Purdue University, West Lafayette, Indiana, USA, 2019.

[8] W. I. Futterman, "Dispersive body waves," *Journal of Geophysical Research (1896–1977)*, vol. 67, no. 13, pp. 5279–5291, 1962. DOI: 10.1029/JZ067i013p05279.

[9] Y. Wang, *Seismic Inverse Q Filtering*. Oxford, UK: Blackwell Publishing, 2008.

[10] B. Ursin and T. Toverud, "Comparison of Seismic Dispersion and Attenuation Models," *Studia Geophysica et Geodaetica*, vol. 46, pp. 293–320, 2002.

[11] H. Kolsky, "Stress waves in solids," *Journal of Sound and Vibration*, vol. 1, no. 1, pp. 88–110, 1964. DOI: 10.1016/0022-460X(64)90008-2.